Cai *et al. Animal Diseases* (2024) 4:22
https://doi.org/10.1186/s44149-024-00128-9

Animal Diseases

SHORT COMMUNICATION

Open Access

Overexpression of EspL inhibits autophagy and antigen presentation to promote the intracellular survival of *Mycobacterium tuberculosis* avirulent strains

Luxia Cai[1], Yingying Lei[1], Tianyi Xie[1], Yiling Liu[1], Yutong Fan[1], Bing Yang[1], Shuang Dong[1], Gang Cao[1,2,3,4,5,6*] and Xi Chen[1*]

Abstract

Mycobacterium tuberculosis (*Mtb*) employs multiple mechanisms, such as phagocytosis and autophagy, to evade innate immune clearance and establish infection. In the present study, we identified the ESX-1 secretion-associated protein EspL, which promotes *Mtb* survival by inhibiting phagosome maturation and autophagy initiation. EspL knockout decreased *Mtb* intracellular survival, while EspL overexpression increased bacterial survival by interfering with phagocytosis and autophagy. EspL interacts with ULK1 and promotes its phosphorylation at Ser^{757}, leading to the inhibition of autophagy initiation. Additionally, overexpression of EspL reduced antigen presentation and T-cell responses both in vitro and in vivo. Our findings revealed that EspL interferes with autophagy and antigen presentation by suppressing ULK1 activation. These insights provide a novel understanding of *Mtb* pathogenicity.

Keywords *Mycobacterium tuberculosis*, EspL, Pathogenicity, Autophagy, Antigen presentation, T-cell responses

Main text

Mycobacterium tuberculosis (*Mtb*), the causative agent of tuberculosis (TB), is primarily phagocytized and restricted by macrophages (Chen et al. 2021; Rahman et al. 2022). The engulfed bacteria are transported to lysosomes for degradation (Flannagan et al. 2012). *Mtb* escapes from phagosomes to the cytosol and triggers autophagy (Gutierrez et al. 2004; Poirier and Av-Gay 2015; Reheman et al. 2023), which selectively targets escaped bacteria for lysosomal degradation (Franco et al. 2017; Manzanillo et al. 2013). The degraded bacterial debris facilitates MHC II antigen presentation to activate T-cell responses against *Mtb* infection (Dengjel et al. 2005; Schmid et al. 2007).

EspL promotes Mtb survival in macrophages and mice

The *Mtb* ESX-1 secretion system and its associated proteins have been reported to inhibit phagosome

Handling editor: Zhong Peng.

*Correspondence:
Gang Cao
caog@siat.ac.cn
Xi Chen
chenxi419@mail.hzau.edu.cn
[1] National Key Laboratory of Agricultural Microbiology, College of Veterinary Medicine, Huazhong Agricultural University, Wuhan, China
[2] Bio-Medical Center, Huazhong Agricultural University, Wuhan, China
[3] College of Informatics, Huazhong Agricultural University, Wuhan, China
[4] Cooperative Innovation Center for Sustainable Pig Production, Huazhong Agricultural University, Wuhan, China
[5] Key Laboratory of Development of Veterinary Diagnostic Products, Ministry of Agriculture, Huazhong Agricultural University, Wuhan, China
[6] Present address: Faculty of Life and Health Sciences, Shenzhen Institute of Advanced Technology, Chinese Academy of Sciences, Shenzhen, China

maturation and autophagy (Chen et al. 2013; Huang and Bao 2016; Mehra et al. 2013; Romagnoli et al. 2012; Wong 2017; Xu et al. 2007). In the present study, we found that the ESX-1 secretion-associated protein EspL interacts with multiple proteins related to autophagy and phagocytosis pathways (Fig. 1A). To investigate whether EspL affects the pathogenicity of *Mtb*, the *EspL*-OE (*EspL* gene-overexpressing) *Mtb* H37Ra strain and the Δ*EspL* (*EspL* gene-deletion) *Mtb* H37Ra strain were constructed (Fig. S1A-S1C). The growth curves showed that neither *EspL*-OE nor Δ*EspL* affected mycobacterial proliferation in vitro (Fig. 1B). The number of viable intracellular bacteria was significantly greater in the *EspL*-OE strain and significantly lower in the Δ*EspL* strain than in the wild-type H37Ra strain (Fig. 1C, Fig. S1D), indicating that EspL is important for *Mtb* virulence in macrophages (Sala et al. 2018).

Furthermore, the role of EspL in a mouse model were investigated. There was no significant difference in the survival of any of the strains at one week postinfection. Nevertheless, the survival of Δ*EspL* strain was significantly decreased in the mouse lungs compared to that of the wild-type strain at two weeks postinfection (Fig. 1D). In mouse spleens, the ΔEspL strain showed significantly decreased survival compared to the wild-type strain at 2 weeks postinfection but not at one week postinfection. In comparison, the survival of the *EspL*-OE strain was not significantly different from that of the wild-type strain at both one and two weeks postinfection (Fig. 1E). The histological examination results showed that the *EspL*-OE strain caused more cellular and inflammatory infiltration in the lungs and spleens of infected mice than did the wild-type or Δ*EspL* strains (Fig. 1F and G, Fig. S1E and S1F). An excessive host inflammatory response kills bacteria and deprives them of their niche by inducing cell death (Amaral et al. 2021), resulting in slightly but not significantly increased survival of the *EspL*-OE strain in mouse lungs and spleens. Therefore, EspL is a potential virulence protein that participates in *Mtb* survival both in vitro and in vivo and likely plays a critical role in the early stages of infection.

Overexpression of EspL inhibits phagosome maturation and autophagy initiation

Phagocytosis and autophagy are crucial for the restriction of intracellular *Mtb* (Deghmane et al. 2007; Franco et al. 2017). However, virulent *Mtb* proteins can subvert these cellular processes (Paz et al. 2010; Vergne et al. 2005). To investigate whether EspL interferes with phagocytosis and autophagy, we infected macrophages with *EspL*-OE, Δ*EspL* or wild-type strains and immunostained them for the phagosome marker Rab7 (Stroupe 2018), the autophagosome marker LC3 (Liang et al. 2017), and the lysosome marker LysoTracker for colocalization (Fig. 2A). Compared with those of the wild-type strain, the colocalization of Rab7 or LysoTracker with the Δ*EspL* strain significantly increased, while the colocalization of both markers with the *EspL*-OE strain significantly decreased (Fig. 2B-E), indicating that EspL arrests the maturation of phagolysosomes (Brodin et al. 2010).

Furthermore, the colocalization of both *EspL*-OE and Δ*EspL* strains with LC3 was significantly decreased compared to that of the wild-type strain (Fig. 2F and G), and the western blotting results were consistent (Fig. 2H and I) because the Δ*EspL* strain could be compromised in virulence and cannot intrinsically induce autophagy (Sala et al. 2018). Selective autophagy can be induced by damaged membranes or cytosolic bacteria (Gomes and Dikic 2014; Liang et al. 2017; Turco et al. 2020; Zaffagnini and Martens 2016). However, the attenuated Δ*EspL* strain cannot disrupt the phagosomal membrane to trigger autophagy. In contrast, the H37Ra wild-type strain effectively escapes from phagosomes (McDonough et al. 1993), initiating the autophagy pathway. Nonetheless, compared with the wild-type strain, the *EspL*-OE strain exhibited a significantly reduced level of autophagy. Therefore, we concluded that EspL overexpression inhibits mycobacterium-induced autophagy.

Mtb proteins such as Rv0790c, PknG and PE_PGRS47 have been reported to inhibit autophagic flux (Fang et al. 2022; Ge et al. 2022; Strong et al. 2021). To investigate whether EspL influences changes in autophagic flux, THP-1 cells were treated with the autophagy–lysosome inhibitor bafilomycin A1 (Franco et al. 2017). Western

(See figure on next page.)

Fig. 1 EspL promotes *Mtb* survival in macrophages and mice. **A** Filtered interaction network between EspL and host proteins. The gray node represents EspL. The blue, red and green nodes represent host proteins related to autophagy, phagocytosis and both autophagy and phagocytosis, respectively. **B** Growth curves of the wild-type, *EspL*-OE and Δ*EspL* H37Ra strains in 7H9 broth. **C** Intracellular survival assay. The experiment was repeated three times. One representative result is shown. **D**, **E** Animal experiment. **F** Representative H&E (hematein and eosin)-stained lung sections of mice at week one. The arrows indicate inflammatory infiltration. Scale bars, 200 μm. **G** Representative H&E (hematein and eosin)-stained spleen sections of mice at week two. The arrow indicates inflammatory infiltration and obscure boundaries of the red and white pulp. Scale bars, 200 μm. The data in **B**, **C**, **D**, and **E** are presented as the means ± s.e.m.ss and were analyzed via two-way ANOVA. $P > 0.05$, not significant (ns); *$P < 0.05$; **$P < 0.01$; ***$P < 0.001$; ****$P < 0.0001$

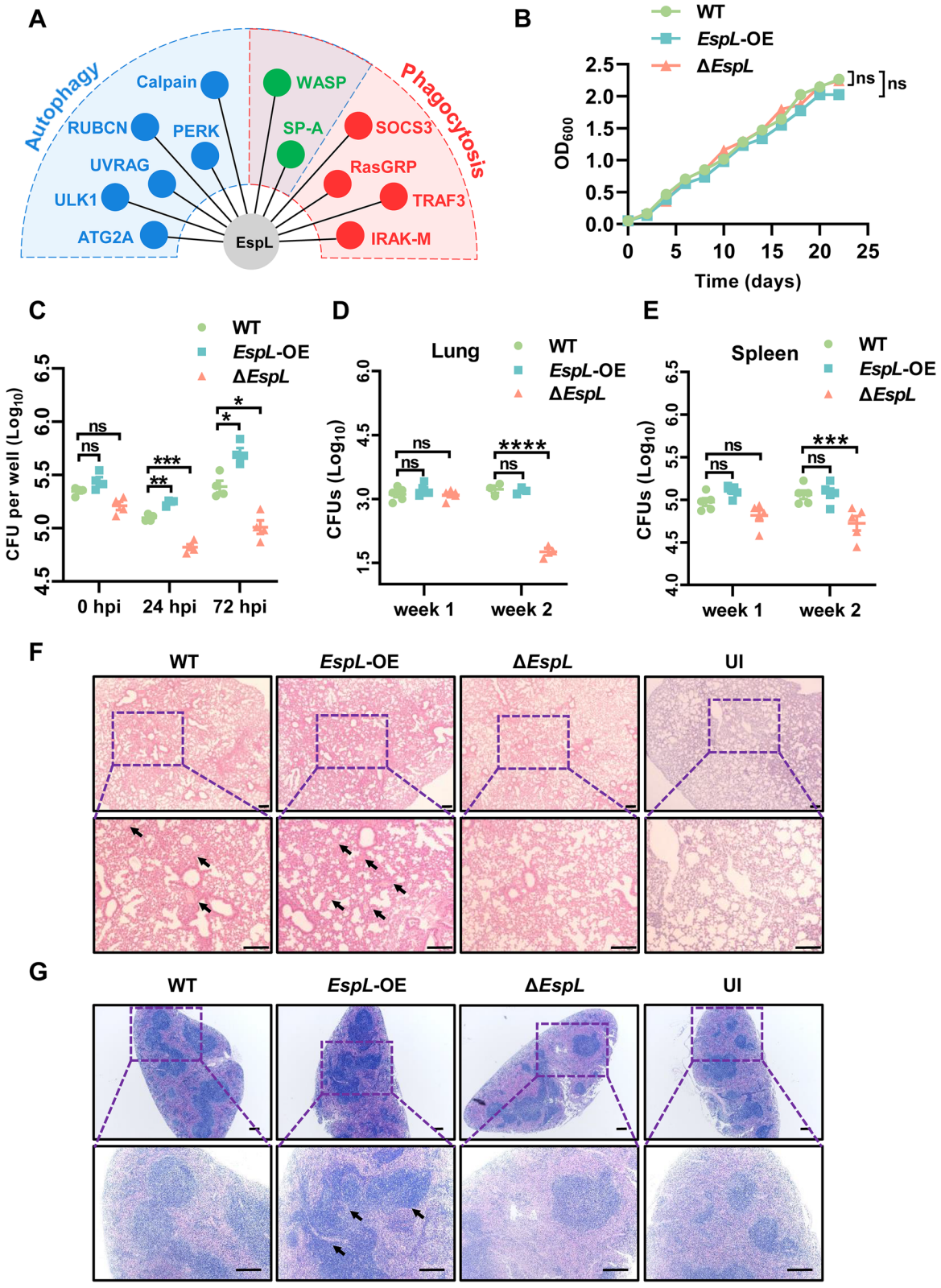

Fig. 1 (See legend on previous page.)

blotting revealed significantly increased LC3 II accumulation in uninfected and wild-type and Δ*EspL* strain-infected cells after bafilomycin A1 treatment (Fig. S2A and S2B). However, the LC3 II protein level in the *EspL*-OE strain-infected cells did not significantly differ in the presence of bafilomycin A1, indicating that EspL effectively blocked autophagic flux (Fig. S2B). Furthermore, the LC3 II expression of untreated cells were subtracted from that of bafilomycin A1-treated cells to evaluate LC3 II degradation. A significantly decreased LC3 II degradation was found in the *EspL*-OE strain-infected cells compared to the wild-type strain-infected cells, indicating a decrease in autophagic flux (Fig. S2C). These data suggest that EspL overexpression interferes with both phagocytosis and autophagy pathways.

EspL inhibits autophagy initiation by increasing ULK1 phosphorylation

To investigate the proteins that interact with EspL, PPI network was double-checked by (Yang et al. 2018) with yeast two-hybrid (Y2H) and bimolecular fluorescence complementation (BiFC) assays. The results showed that ULK1, ATG2A and RUBCN had obvious effects on yeast cell growth (Fig. 3A) and apparent signals of red fluorescence (Fig. 3B), suggesting that they interact with EspL. Autophagy is regulated by a group of autophagy-related (ATG) proteins (Huang and Brumell 2014; Suzuki et al. 2013; Yu et al. 2018). Three proteins involved in the initiation (ULK1), nucleation and extension (ATG2A), and maturation (RUBCN) stages of autophagy were identified (Fig. 3C). Then, ULK1, ATG2A and RUBCN were silenced in macrophages and detected autophagy levels. Data showed that RUBCN- or ATG2A-knockdown cells accumulated more LC3 II than did control cells (Fig. S3A and S3C), which is consistent with the roles of these two proteins in autophagy (Gomez-Sanchez et al. 2018; Matsunaga et al. 2009; Sun et al. 2011; Tamura et al. 2017; Velikkakath et al. 2012). However, the downregulation of RUBCN or ATG2A did not affect the differences in LC3 II expression between the wild-type and *EspL*-OE strains (Fig. S3A-S3D). Furthermore, the knockdown of ULK1 in macrophages was confirmed (Fig. S3E-S3G). ULK1 deficiency impaired the accumulation of LC3 II and rescued the reduced LC3 II level in macrophages during *EspL*-OE strain infection (Fig. 3D and E), suggesting that ULK1 is required for the ability of EspL to inhibit autophagy. As the activity of ULK1 is highly regulated by phosphorylation and other modifications (Kim et al. 2011; Zachari and Ganley 2017), the influence of EspL on the phosphorylation state of ULK1 was evaluated. Compared to infection with the wild-type strain, infection with the *EspL*-OE strain led to more Ser^{757}-phosphorylated ULK1 (Fig. 3F and G), suggesting a suppressive effect on ULK1. However, the amount of total ULK1 remained the same (Fig. 3H and I). Since mTORC1 negatively regulates autophagy initiation by phosphorylating ULK1 at Ser^{757}, the increased phosphorylation of ULK1 at Ser^{757} indicates a decrease in autophagy (Kim et al. 2011; Rabanal-Ruiz et al. 2017). These data suggest that EspL interacts with ULK1 and increases its phosphorylation at Ser^{757} to inhibit autophagy initiation.

Overexpression of EspL suppresses MHC II antigen presentation and T-cell responses

To investigate whether EspL suppresses MHC II antigen presentation during *Mtb* infection, an in vitro experiment was performed in which BMDCs were infected with different *Mtb* strains and then cocultured with antigen-sensitized splenocytes (Fig. 4A). The flow cytometry results showed that compared with infection with the wild-type strain, infection with the *EspL*-OE strain led to a significant decrease in the percentage of MHC II^+ $CD11c^+$ BMDCs (Fig. 4B and C). The expression of MHC II molecules on the surface of BMDCs infected with the *EspL*-OE strain was also significantly lower than that on the surface of BMDCs infected with the wild-type strain (Fig. 4D), indicating that EspL has an inhibitory effect on the antigen presentation ability of BMDCs.

(See figure on next page.)

Fig. 2 EspL inhibits phagosome maturation and autophagy. **A** Schematic model of the phagocytosis and autophagy pathways. **B** Confocal microscopy analysis of the colocalization of *Mtb* with Rab7. THP-1 cells were infected with the wild-type, *EspL*-OE or Δ*EspL* H37Ra strain (green) at an MOI of 10 for 24 h and stained with an anti-Rab7 antibody (red). DAPI was used to stain the nuclei (blue). Scale bars, 20 μm. The experiment was repeated two times. **C** Quantification of the colocalization of the *Mtb* strains with Rab7. **D** Confocal microscopy analysis of the colocalization of *Mtb* with LysoTracker. THP-1 cells were infected with the wild-type, *EspL*-OE or Δ*EspL* H37Ra strains (green) at an MOI of 10 for 24 h and stained with LysoTracker (red). Hoechst was used to stain the nuclei (blue). Scale bars, 20 μm. The experiment was repeated two times. **E** Quantification of the colocalization of *Mtb* strains with LysoTracker. **F** Confocal microscopy analysis of the colocalization of *Mtb* with LC3. THP-1 cells were infected with the wild-type, *EspL*-OE or Δ*EspL* H37Ra strains (green) at an MOI of 10 for 24 h and stained with an anti-LC3 antibody (red). DAPI was used to stain the nuclei (blue). Scale bars, 20 μm. The experiment was repeated three times. **G** Quantification of the colocalization of *Mtb* strains with LC3. **H** Immunoblot analysis of LC3 I/II expression in THP-1 cells infected with the wild-type, *EspL*-OE or Δ*EspL* H37Ra strains. The experiment was repeated three times. **I** The ratio of the intensities of the LC3 II and GAPDH bands. The data in **C**, **E**, **G**, **I** are presented as the means ± s.e.m.ss and were analyzed *via* one-way ANOVA. $P > 0.05$, not significant (ns); $^*P < 0.05$; $^{**}P < 0.01$; $^{***}P < 0.001$; $^{****}P < 0.0001$

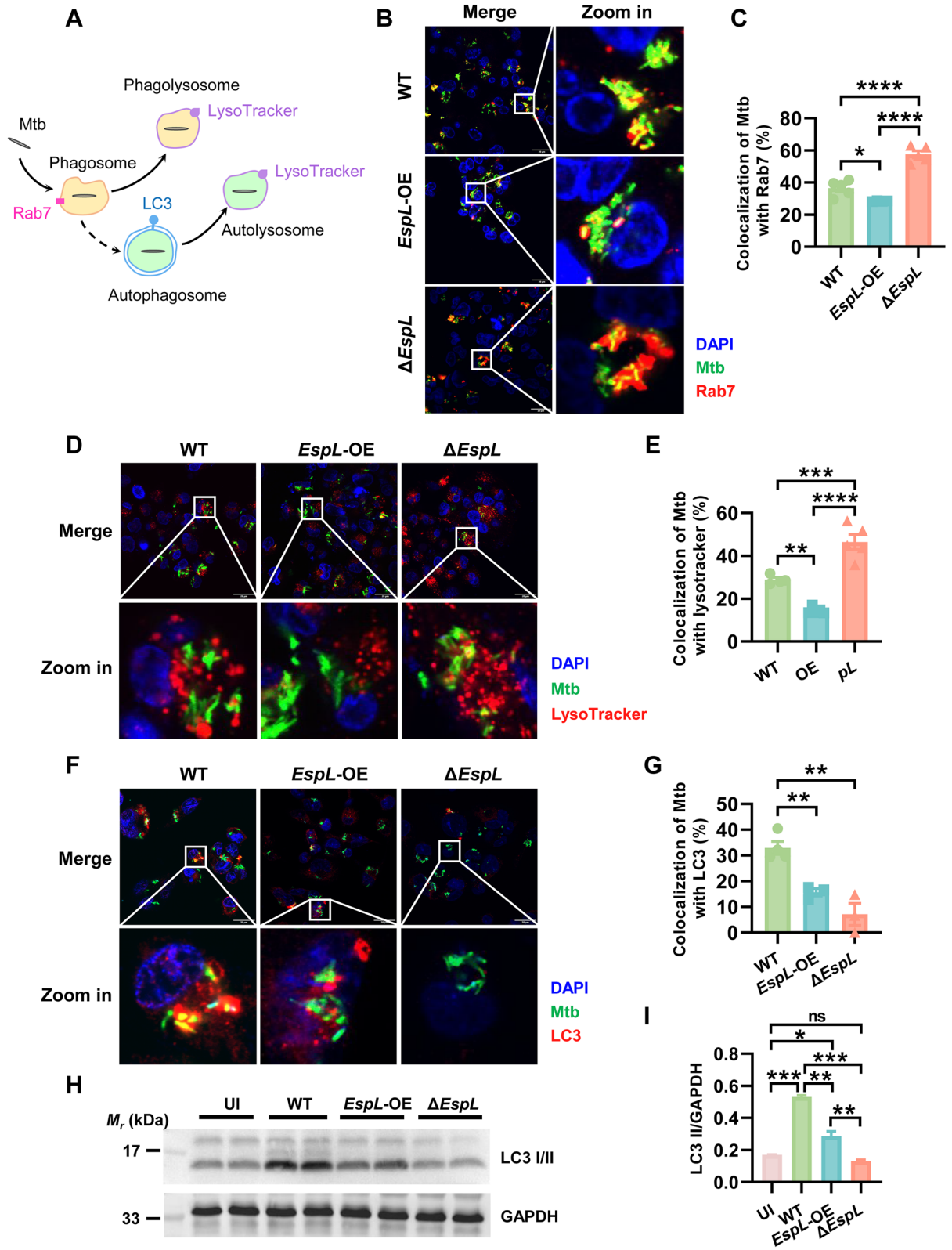

Fig. 2 (See legend on previous page.)

We then examined whether these *Mtb*-infected BMDCs had different capacities for antigen presentation to T cells by an IFN-γ release assay (Saini et al. 2016). Compared with wild-type strain-infected BMDCs, *EspL*-OE strain-infected BMDCs were defective in stimulating T-cell responses (Fig. 4E). Unexpectedly, compared with the wild-type strain, the Δ*EspL* strain demonstrated no improvement in MHC II expression or T-cell responses, and the IFN-γ release of the Δ*EspL* strain-infected group was comparable to that of the uninfected group (Fig. 4B-E). This finding suggested that EspL is necessary for activating T-cell responses and that the Δ*EspL* strain cannot induce T-cell activation. *EspL* is located within the ESX-1 gene locus and encodes a protein associated with ESX-1 secretion. Knockout of *EspL* disrupts the function of the ESX-1 system and impairs the secretion of various effector proteins (Sala et al. 2018). As a result, the Δ*EspL* strain displayed significantly reduced virulence and an inability to express multiple antigenic proteins required for stimulating T-cell responses.

To further assess antigen presentation in vivo, C57BL/6 mice were infected with the wild-type, *EspL*-OE, and Δ*EspL* H37Ra strains, and mouse spleens were collected on day 28 postinfection (Fig. 4F). T-cell responses were measured by restimulating splenocytes with wild-type H37Ra-infected BMDCs. There was no significant difference in the proportions of $CD4^+$ or $CD8^+$ T cells among the splenocytes of the mice infected with the three indicated strains (Fig. 4G-I). However, the T-cell responses specific for *Mtb* antigens displayed a prominent distinction, as illustrated by a significant decrease in the amount of IFN-γ released by the splenocytes of mice infected with the *EspL*-OE strain compared to that released by the splenocytes of mice infected with the wild-type strain (Fig. 4J). Since autophagy is beneficial for MHC II-mediated antigen presentation (Baena and Porcelli 2009; Ernst 2012), we concluded that EspL overexpression may hinder MHC II-mediated antigen presentation and subsequent T-cell responses through the inhibition of autophagy.

Our data identified EspL as a virulence protein that promotes *Mtb* survival both in vitro and in vivo. EspL contributes to *Mtb* evasion of both phagocytosis and autophagy pathways. EspL overexpression inhibits autophagy by interacting with ULK1 and reducing its activation. EspL overexpression also suppresses antigen presentation, which may be due to the inhibitory effect of EspL on autophagy. Our data may provide insights into *Mtb* pathogenicity and facilitate the design of anti-*Mtb* vaccines.

Methods

Antibodies and reagents

The primary antibodies used in this study were anti-LC3B (CST, #3868, 1:300 for immunostaining and 1:1000 for western blotting), anti-Rab7 (Santa Cruz, sc-10767, 1:50 for immunostaining), anti-GAPDH (ABclonal, A19056, 1:1000 for western blotting), anti-β-Actin (ABclonal, AC004, 1:1000 for western blotting), anti-RUBCN (MBL, M170-3, 1:1000 for western blotting), anti-ATG2A (Proteintech, 23226–1-AP, 1:1000 for western blotting), anti-ULK1 (CST, #8054 T, 1:1000 for western blotting), anti-phospho-ULK1 (Ser757) (CST, #14202, 1:1000 for western blotting), anti-I-A/I-E-APC (BioLegend, 107614, 0.1 μg for FACS), anti-CD11c-PC7 (BioLegend, 117318, 0.1 μg for FACS), anti-CD3-PB (BioLegend, 100214, 0.1 μg for FACS), and anti-CD4-FITC (BioLegand, 100509, 0.1μg for FACS) and anti-CD8-APC (BioLegand, 100711, 0.1μg for FACS). The secondary antibodies used were: HRP goat anti-rabbit IgG (ABclonal, AS014, 1:1000 for western blotting), HRP goat anti-mouse IgG (ABclonal, AS003, 1:1000 for western blotting), Alexa Fluor® 555 goat anti-rabbit IgG (Invitrogen, A21429, 1:600 for immunostaining). LysoTracker (C1046), DAPI (C1005), and Hoechst 33342 (C1027) were purchased from Beyotime. A mouse IFN-γ ELISA kit (RK00019), active recombinant mouse GM-CSF protein (RP01206), and active recombinant mouse IL-4 protein (RP01161) were purchased from ABclonal. Bafilomycin A1 (#54645) was purchased from CST.

(See figure on next page.)

Fig. 3 EspL inhibits autophagy initiation by increasing ULK1 phosphorylation. **A** Verification of the interaction of EspL with ULK1, RUBCN and ATG2A by Y2H assay. The empty pmAD and pmBD vectors were used as negative controls. The Y2H experiment was repeated two times. **B** Verification of the protein–protein interactions by BiFC assay. The empty ΔFos and ΔJun vectors were used as negative controls. Scale bars, 100 μm. The BiFC experiment was repeated three times. **C** Schematic model for the roles of ULK1, ATG2A and RUBCN in the autophagy process. **D** Immunoblot analysis of LC3 I/II expression in shNC or *ULK1*-KD THP-1 cells infected with the wild-type or *EspL*-OE H37Ra strains (MOI = 10) for 24 h. The experiment was repeated two times. **E** The ratio of the intensity of the LC3 II band to that of the GAPDH band. **F** Immunoblot analysis of Ser^{757}-phosphorylated ULK1 in THP-1 cells infected with the wild-type or *EspL*-OE H37Ra strains (MOI = 10) for 24 h. The experiment was repeated two times. **G** The ratio of the intensities of phosphorylated ULK1 to those of the GAPDH bands. **H** Immunoblot analysis of total ULK1 in THP-1 cells infected with the wild-type or *EspL*-OE H37Ra strains (MOI = 10) for 24 h. **I** The ratio of the intensities of total ULK1 to those of the GAPDH bands. The data in **E**, **G**, **I** are presented as the means ± s.e.m.ss. **E** was analyzed via two-way ANOVA. **G** and **I** were analyzed via one-way ANOVA. $P > 0.05$, not significant (ns); $^*P < 0.05$; $^{**}P < 0.01$

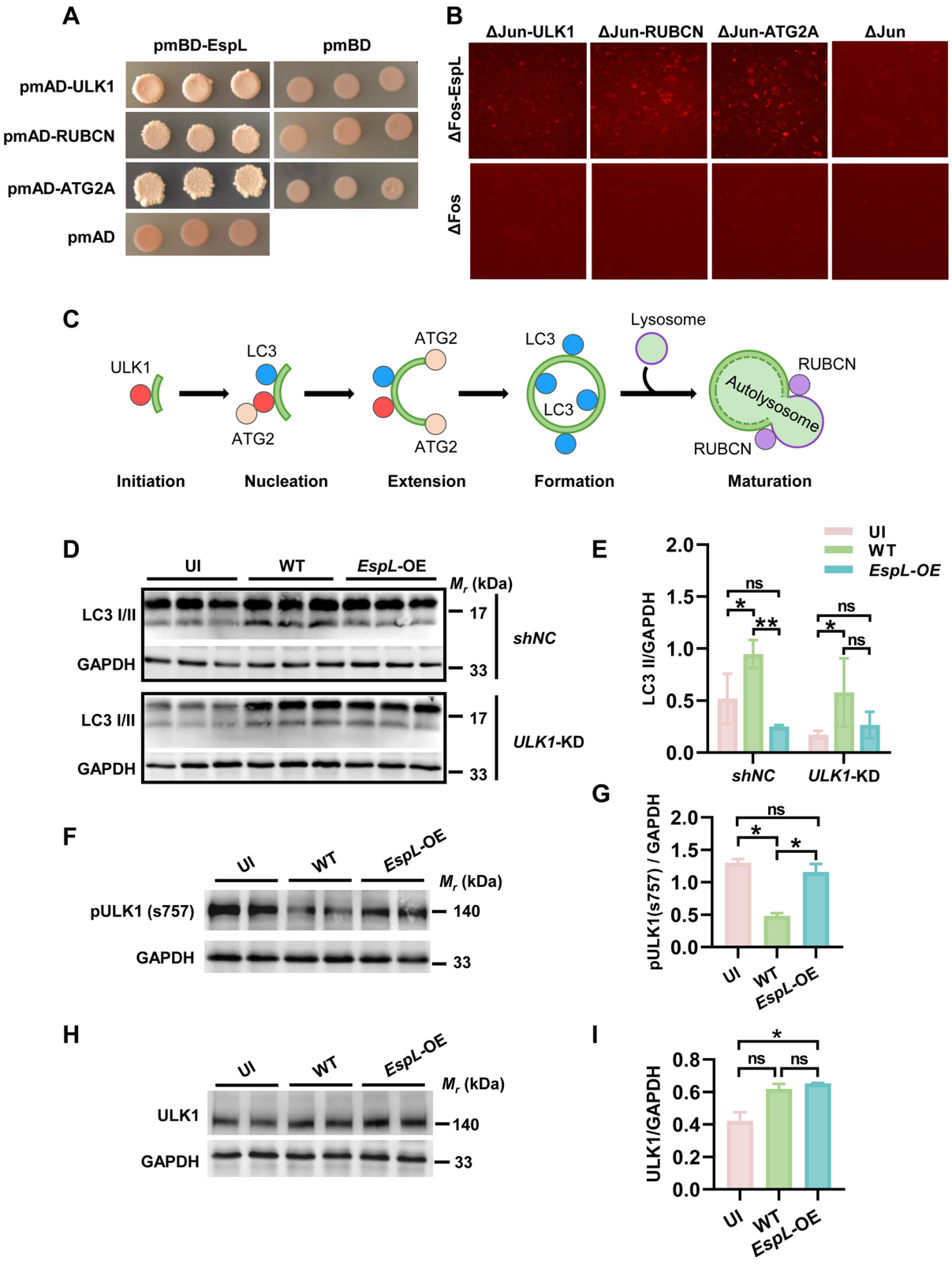

Fig. 3 (See legend on previous page.)

Bacterial strains and culture conditions

The wild-type *Mtb* (strain H37Ra, ATCC 25177) and the overexpressing and knockout strains were cultured at 37 ℃ in Difco™ Middlebrook 7H9 broth (BD, 271310) or on 7H11 agar (BD, 283810) supplemented with 10% oleic acid albumin dextrose catalase (OADC, BD, 211886), 0.5% glycerol and 0.05% Tween-80. For confocal microscopy, *Mtb* H37Ra strains were transformed with a pMV261-eGFP plasmid and maintained in the presence of kanamycin (25 μg/mL). The overexpressing strain (*EspL*-OE) was generated by transforming pMV261-EspL-eGFP into wild-type H37Ra. For the knockout strain (Δ*EspL*), the *EspL* gene was replaced by the *hyg* gene via the phage-mediated allelic exchange method (Jain et al. 2014). Colonies were screened for hygromycin resistance (100 μg/mL) and identified by PCR to confirm gene deletion.

Cell culture and infection

THP-1 cells (ATCC TIB-202) were cultured in RPMI-1640 medium (Gibco, C11875500BT) supplemented with 10% fetal bovine serum (FBS, Gibco, 10099141C), 100 units/mL penicillin and 100 μg/mL streptomycin (Gibco, 15140122) at 37°C with 5% CO_2.

BMDCs were prepared as previously described (Lutz et al. 1999). Briefly, bone marrow was obtained from the tibiae and femurs of six-week-old female C57BL/6 mice. Cells were seeded in 6-well tissue culture plates in RPMI-1640 medium supplemented with 10% FBS, 100 units/mL penicillin, 100 μg/mL streptomycin, 20 ng/mL GM-CSF, and 10 ng/mL IL-4. Half of the cell culture medium was removed every two days, and fresh medium was added. Immature BMDCs were harvested on day 10, followed by treatment with 50 ng/mL lipopolysaccharide (LPS) for 24 h to stimulate mature BMDCs. Mature BMDCs were seeded at 2×10^4 cells per well and infected with the wild-type H37Ra strain at a multiplicity of infection (MOI) of 5 for 6 h. The cells were washed with phosphate-buffered saline (PBS) three times and then treated with 100 μg/mL gentamicin for 1 h to stop infection.

HEK293T cells (ATCC CRL-3216™) were maintained in Dulbecco's modified Eagle medium (DMEM, Gibco, C11995500BT) supplemented with 10% FBS, 100 units/mL penicillin, and 100 μg/mL streptomycin at 37°C with 5% CO_2.

Intracellular colony-forming units

THP-1 cells were seeded at 2.5×10^5 cells per well in 24-well plates for 24 h in RPMI-1640 medium supplemented with PMA (Phorbol 12-Myristate 13-Acetate, Sigma–Aldrich, 19–144) and then infected with *Mtb* H37Ra (MOI = 5) for 6 h. Then, the cells were washed three times with prewarmed PBS and treated with gentamicin (100 μg/mL) for 1 h. The cells were lysed with 500 μl of sterile 0.1% Tween 80 for 10 min at the indicated time points. The cell lysates were diluted, and 50 μl of the diluted lysates were plated on 7H11 agar plates to count the number of CFUs.

Immunostaining and confocal microscopy

THP-1 cells were seeded onto coverslips and infected with *Mtb* H37Ra strains (MOI = 10). The cells were fixed with cold 100% methanol for 5 min at 24 h postinfection (hpi), rinsed three times with PBS and blocked with 10% goat serum for 1 h at room temperature (RT). Primary antibodies (anti-Rab7 or anti-LC3) were applied to the cells at 4 °C overnight, followed by incubation with the secondary antibody Alexa Fluor® 555-conjugated goat anti-rabbit IgG for 1 h at RT. DAPI (1:5000) was used to stain the nucleus. The cells were washed three times with PBS and then mounted onto microscope slides. For the immunostaining of lysosomes, cells were seeded in Petri dishes (Biosharp, BS-15-GJM) and incubated with LysoTracker for 5 min at 37°C, followed by staining with Hoechst for 5 min at 37°C. The images were obtained with an Olympus FV1000 confocal microscope and analyzed with FV10 ASW Imaging Software (V. 4.2, Olympus). The colocalization of *Mtb* with Rab7, LC3 or LysoTracker was quantified by counting 300 bacteria.

(See figure on next page.)

Fig. 4 EspL suppresses MHC II antigen presentation and T-cell responses. **A** Schematic model for the assessment of antigen presentation by BMDCs in vitro. **B** BMDCs were infected with the wild-type, *EspL*-OE or Δ*EspL* H37Ra strains and stained with anti-MHC II and anti-CD11c antibodies for flow cytometry. **C** Quantification of MHC II^+ and $CD11c^+$ cells. **D** Mean fluorescence intensity (MFI) of MHC II^+ molecules. **E** IFN-γ release assay. The infected BMDCs were cocultured with the splenocytes of wild-type H37Ra-infected mice for 3 d, and the cell culture supernatant was collected for ELISA. **F** Schematic model for the assessment of T-cell responses in vivo. **G** C57BL/6 mice ($n = 5$ per group) were intravenously infected with the wild-type, *EspL*-OE or Δ*EspL* H37Ra strains (1×10^6 CFU per mouse). The splenocytes were harvested at 28 dpi and stained with anti-CD4 and anti-CD8 antibodies for flow cytometry analysis. **H**, **I** Quantification of $CD4^+$ T cells and $CD8^+$ T cells. **J** IFN-γ release assay. The splenocytes of infected mice were restimulated with wild-type H37Ra-infected BMDCs, and the IFN-γ concentration in the supernatant was detected by ELISA. The experiments in **B-E** and **G-J** were repeated two times. $P > 0.05$, not significant (ns); $^*P < 0.05$; $^{**}P < 0.01$; $^{***}P < 0.001$; $^{****}P < 0.0001$ (one-way ANOVA)

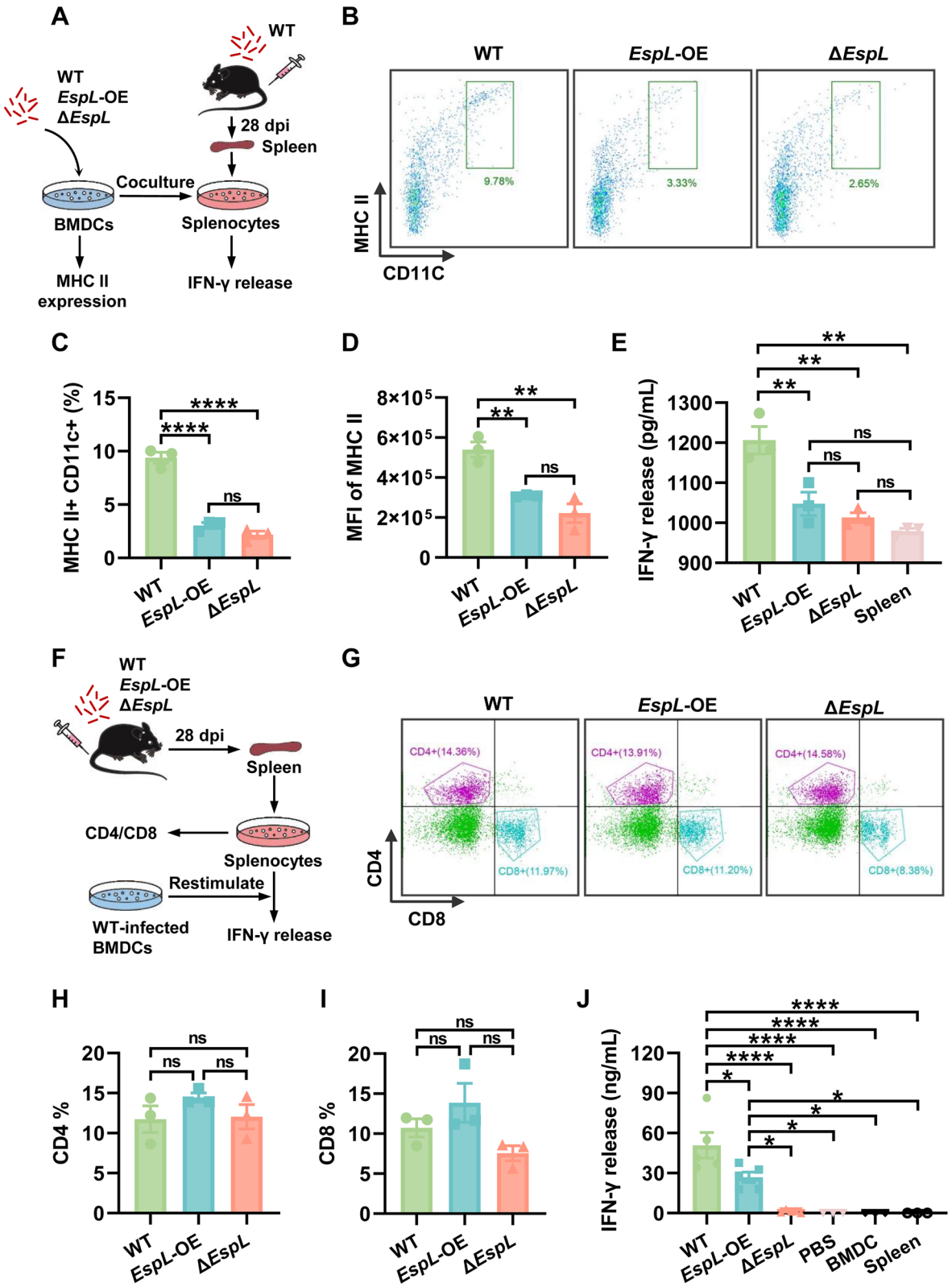

Fig. 4 (See legend on previous page.)

Yeast two-hybrid (Y2H) assay

Y2H was performed using the GAL4 Y2H system (Lei et al. 2021). *EspL* was cloned and inserted into the pmBD vector, which was subsequently transformed into the yeast strain Y2HGold. The host genes *RUBCN*, *ATG2A* and *ULK1* were cloned and inserted into the pmAD vector, which was subsequently transformed into the yeast strain Y187. Then, Y187 cells containing pmAD constructs were mated with Y2HG-old cells containing pmBD-*EspL* and selected on minimal media lacking leucine and tryptophan. Protein–protein interactions were identified by spotting the mated yeast cells onto synthetic dropout media lacking leucine, tryptophan, histidine, and adenine (SD/Leu^{-} Trp^{-} His^{-} Ade^{-}) and growing for 5–7 d at 30°C.

Bimolecular fluorescence complementation (BiFC) assay

BiFC plasmids were constructed by cloning *EspL* into the ΔFos vector and cloning *RUBCN*, *ATG2A* and *ULK1* into the ΔJun vector. For transfection, 2×10^5 HEK293T cells per well were seeded in a 24-well plate overnight. Then, 1 μg of BiFC plasmid per well was transfected into HEK293T cells using the polyethyleneimine method for three days. Images were obtained under a fluorescence microscope.

Western blotting

THP-1 cells were lysed in RIPA buffer (Beyotime, P0013B) supplemented with 1 mM phenylmethylsulfonyl fluoride (PMSF, Biosharp, BL507A). Proteins were quantified by a BCA assay (Abbkine, KTD3001) and subjected to sodium dodecyl sulfate–polyacrylamide gel electrophoresis (SDS–PAGE), followed by transfer to polyvinylidene fluoride (PVDF) membranes (Bio-Rad, 1620177). After blocking with 5% skim milk in Tris-buffered saline with Tween (TBST) or with 5% bovine serum albumin (BSA) in TBST for 1 h, the membrane was incubated with primary antibodies overnight at 4°C and then incubated with secondary antibodies for 1 h at RT. The membrane was developed with an enhanced chemiluminescence (ECL) substrate (Bio-Rad, 1705060) and exposed with a GBox XT4 chemiluminescence imager (Gene Company). The quantification of specific bands was performed by Image-Pro Plus V. 6.0.

Construction of gene knockdown cell lines

Scramble and targeted shRNAs were designed using an online tool (https://portals.broadinstitute.org/gpp/public/) (GPP Web Portal, 2021) (shown in Table S1) and inserted into the pLKO.1-mCherry vector. pLKO.1-shRNAs were cotransfected with pMD.2G and pSPAX into HEK293T cells for three d to package lentiviruses. The cell culture supernatants were filtered through 0.22 μm filters (Millipore, SLGPR33RB) and incubated with lentivirus solution (Biodragon, BF06205) overnight at 4°C. Viral particles were acquired by centrifugation and added to wild-type THP-1 cells. At 48 h postinfection (hpi), the lentivirus-infected cells were collected and resuspended in fresh RPMI-1640 medium supplemented with 10% FBS and 2 μg/mL puromycin (InvivoGen, 58-58-2). The cells were subsequently purified with puromycin for two weeks.

qPCR analysis

Total RNA from the THP-1 cell line was isolated with RNAiso Plus reagent (Takara, 9109). For the total RNA extraction of mycobacteria, 0.1 mm glass beads were added and centrifuged on a tissue crusher before applying the RNAiso Plus reagent. Reverse transcription of RNA was conducted with ABScript III RT Master Mix (ABclonal, RK20428). qPCR was performed with 2×Universal SYBR Green Fast qPCR Mix (ABclonal, RK21203) on a QuantStudio 3 system (Applied Biosystems). The relative expression of the target gene was normalized to that of *Gapdh* for human genes or to that of *SigA* for mycobacterial genes using the $2^{-\Delta\Delta Ct}$ method. The primers used for qRT–PCR are shown in Table S1.

Animal experiments

The animal experiment was carried out under the administration of animal care and usage for research by the Ministry of Health in China. The animals were raised in specific-pathogen-free rooms. All the experiments were approved by the Scientific Ethics Committee of Huazhong Agricultural University (HZAUMO-2023–0189).

Six- to eight-week-old C57BL/6 female mice were purchased from and raised at the Laboratory Animal Center of Huazhong Agricultural University. Animals were randomly assigned to experimental groups of five each. C57BL/6 mice were infected intravenously *via* the tail vein with 1×10^6 CFU per mouse. Mice were euthanized on days 7, 14 and 28 postinfection. Mouse spleens were fixed with 4% paraformaldehyde, paraffin-embedded, sectioned, and subjected to H&E staining for histopathology analysis. The bacterial burdens in the spleens were determined by CFU enumeration. For the isolation of single spleen cells, each spleen tissue sample was forced through a 70 μm cell strainer (Biosharp, BS-70-CS) with a plunger from a 1 mL syringe (BD, 328,421). The splenic erythrocytes were lysed, and the cells were washed twice in Hanks balanced salt solution (HBSS, Biosharp, BL559A) and resuspended in RPMI-1640 media supplemented with 10% FBS. Finally, single-cell suspensions were adjusted to 2×10^5 cells/well for ELISA and 1×10^6 cells/well for flow cytometry.

Fluorescence-activated cell sorting (FACS) analysis

Splenocytes or H37Ra-infected BMDCs were washed twice with FACS buffer (PBS, 2% BSA) and stained with 0.1 μg of fluorochrome-conjugated antibodies in 100 μL of FACS buffer for 1 h at 4°C. The stained cells were washed twice and then resuspended in FACS buffer. The samples were loaded onto a four-color Cytoflex-LX cytometer (Beckman Coulter) for analysis. For BMDCs, anti-CD11c-PC7 and anti-I-A/I-E-APC mAbs were used to evaluate the in vitro antigen presentation ability. For splenocytes, anti-CD3-PB, anti-CD4-FITC and anti-CD8-APC mAbs were applied to analyze the T-cell responses. CytExpert software was used for data analysis and image output.

Analysis of T-cell responses by enzyme-linked immunosorbent assay (ELISA)

In vitro antigen presentation experiment was designed to infect BMDCs with the wild-type, *EspL*-OE, and Δ*EspL* strains, and the ability of infected BMDCs to stimulate splenocytes from wild-type H37Ra-infected mice was tested. In vivo, the antigen presentation process was conducted by infecting C57BL/6 mice with the wild-type, *EspL*-OE, and Δ*EspL* strains and testing the responses of splenocytes from H37Ra-infected mice. In general, BMDCs were infected with H37Ra strains and then cocultured with splenocytes for 3 d. Culture supernatants were collected and analyzed with a mouse IFN-γ ELISA kit (ABclonal, RK00019). Briefly, the samples were diluted and transferred to an antibody-coated 96-well plate for 2 h at 37°C. The plate was washed three times. Biotin-conjugated antibody and HRP-conjugated streptavidin were added in sequence to determine the IFN-γ concentration. The color reaction was developed with tetramethylbenzidine (TMB) as the substrate and stopped with a stop solution. The absorbance of the plates was read at 450 nm and 630 nm. The standard curve was modeled by a 4th-degree polynomial fit based on the concentration of the lyophilized IFN-γ standard.

Abbreviations

BiFC	Bimolecular fluorescence complementation
BSA	Bovine serum albumin
CFU	Colony forming units
ELISA	Enzyme-linked immunosorbent assay
hpi	Hours postinfection
LPS	Lipopolysaccharide
MOI	Multiplicity of infection
Mtb	*Mycobacterium tuberculosis*
OADC	Oleic acid albumin dextrose catalase
PMA	Phorbol 12-Myristate 13-Acetate
PMSF	Phenylmethylsulfonyl fluoride
PPI	Protein–protein interaction
TB	Tuberculosis
TMB	Tetramethylbenzidine
Y2H	Yeast two-hybrid

Supplementary Information

The online version contains supplementary material available at https://doi.org/10.1186/s44149-024-00128-9.

Additional file 1: Figure S1 (A) Analysis of the mRNA expression of *EspL* in wild-type H37Ra and the *EspL*-OE strains. ****$P < 0.0001$ (unpaired *t*-test). (B) Verification of the knockout of the *EspL* gene. Fragment 1 was amplified by EspL-Up1200-F and p0004s-inner-R to confirm the homologous exchange of the left arm; Fragment 2 was amplified by p0004s-inner-F and EspL-Dn1000-R to confirm the homologous exchange of the right arm; Fragment 3 was amplified by EspL-ORF-F and EspL-ORF-R to confirm the knockout of *EspL*; Fragment 4 was amplified by SacB-F and SacB-R to confirm the insertion of *SacB* into *Mtb* genome. The arrow indicated the PCR band of *EspL*. Primers used for PCR verification are listed in Table S1. (C) Schematic model for the principles of homologous exchange and the genomic location of PCR fragments in (B). Red dash lines and purple blocks indicate the position where the homologous exchange has happened. Black dash lines and double-headed arrows indicate the location of 4 PCR fragments. (D) Percentage of viable bacteria in (Fig. 1C). The CFUs at 24 hpi and 72 hpi were divided by the CFUs at 0 hpi to calculate the survival percentage. $P > 0.05$, not significant (ns); *$P < 0.05$; **$P < 0.01$; ***$P < 0.001$; ****$P < 0.0001$ (two-way ANOVA). (E) Representative H&E (hematein and eosin)-stained lung sections of mice in (Fig. 1D) at week 2. Scale bars, 200 μm. (F) Representative H&E (hematein and eosin)-stained spleen sections of mice in (Fig. 1E) at week 1. Scale bars, 200 μm.

Additional file 2: Figure S2 (A) THP-1 cells were infected with the wild-type H37Ra, *EspL*-OE or Δ*EspL* strains at MOI = 10 for 24 h. Bafilomycin A1 (Baf A1, 100 nM) was added 3 hours before cells were harvested for immunoblot analysis of LC3 I/II expression. The experiment was repeated once. (B) The ratio of the intensities of the LC3 II to GAPDH bands in Baf A1-treated and untreated THP-1 cells. $P > 0.05$, not significant (ns); *$P < 0.05$; **$P < 0.01$; ***$P < 0.001$; ****$P < 0.0001$ (two-way ANOVA). (C) The differences of LC3 II intensities between Baf A1-treated and untreated groups. The results indicate the amount of LC3 II degraded in lysosomes. $P > 0.05$, not significant (ns); *$P < 0.05$; **$P < 0.01$; ***$P < 0.001$; ****$P < 0.0001$ (one-way ANOVA).

Additional file 3: Figure S3 (A) shNC or *RUBCN*-KD THP-1 cells were infected with the wild-type H37Ra or *EspL*-OE strains (MOI = 10) and analyzed by western blotting for RUBCN, LC3 and GAPDH. The experiment was repeated two times. One representative image is shown. (B) The ratio of the intensities of LC3 II to GAPDH. (C) shNC or *ATG2A*-KD THP-1 cells were infected with the indicated *Mtb* strains (MOI = 10) and analyzed by western blot for ATG2A, LC3 and GAPDH. The experiment was repeated two times. One representative image is shown. (D) The ratio of the intensities of LC3 II to GAPDH. (E) Detection of ULK1 protein levels in shNC or *ULK1*-KD THP-1 cells by western blotting. The experiment was repeated two times. One representative image is shown. (F) The ratio of the intensities of ULK1 to β-Actin. Numbers above the bars indicate the mean values. (G) Analysis of the *ULK1* mRNA expression in shNC or *ULK1*-KD THP-1 cells. **$P < 0.01$ (unpaired *t*-test).

Additional file 4: Table S1. List of primers used in this study. Table S2. List of plasmids used in this study.

Acknowledgements

We acknowledge the State Key Laboratory of Agricultural Microbiology Core Facility at Huazhong Agricultural University for assistance in conducting the confocal microscopy and flow cytometry experiments. We thank Hu Zhe and Wang Fangkui for their technical help and advice in sample preparation and data analysis.

Authors' contributions

C.X., C.G. and C.L. designed the experiments. L.YY. performed the CFU enumeration and BiFC and Y2H assays. C.L., X.T., L.Y. and F.Y. conducted western blotting, qPCR analysis, construction of knockdown cell lines and confocal microscopy. C.L., L.YY. and Y.B. carried out the animal experiments. C.L. and D.S.

constructed the knockout *Mtb* strains. C.L., C.X. and C.G. wrote the manuscript. L.YY. edited the manuscript and contributed to the arrangement of the figures. C.X. and C.G. are responsible for this work. All authors have read and approved the final version of the manuscript.

Funding
This work was supported by the National Natural Science Foundation of China under grant number U21A20259 and the National Key Research and Development Program of China under grant number 2021YFD1800401.

Availability of data and materials
The relevant data and materials in this article are available and can be requested from the corresponding authors.

Declarations

Ethics approval and consent to participate
All the experiments were approved by the Scientific Ethics Committee of Huazhong Agricultural University (HZAUMO-2023–0189).

Consent for publication
Not applicable.

Competing interests
The authors declare no competing interests. Author Cao Gang was not involved in the journal's review or decisions related to this manuscript.

Received: 16 April 2024 Accepted: 11 June 2024
Published online: 25 June 2024

References

Amaral, E.P., C.L. Vinhaes, D. Oliveira-De-Souza, B. Nogueira, K.M. Akrami, and B.B. Andrade. 2021. The interplay between systemic inflammation, oxidative stress, and tissue remodeling in tuberculosis. *Antioxidants & Redox Signaling* 34 (6): 471–485. https://doi.org/10.1089/ars.2020.8124.

Baena, A., and S.A. Porcelli. 2009. Evasion and subversion of antigen presentation by *Mycobacterium tuberculosis*. *Tissue Antigens* 74 (3): 189–204. https://doi.org/10.1111/j.1399-0039.2009.01301.x.

Brodin, P., Y. Poquet, F. Levillain, I. Peguillet, G. Larrouy-Maumus, M. Gilleron, F. Ewann, T. Christophe, D. Fenistein, J. Jang, et al. 2010. High content phenotypic cell-based visual screen identifies *Mycobacterium tuberculosis* acyltrehalose-containing glycolipids involved in phagosome remodeling. *PLoS Pathogens* 6 (9): e1001100. https://doi.org/10.1371/journal.ppat.1001100.

Chen, J.M., M. Zhang, J. Rybniker, S. Boy-Rottger, N. Dhar, F. Pojer, and S.T. Cole. 2013. *Mycobacterium tuberculosis* EspB binds phospholipids and mediates EsxA-independent virulence. *Molecular Microbiology* 89 (6): 1154–1166. https://doi.org/10.1111/mmi.12336.

Chen, X., X. Cao, Y. Lei, A. Reheman, W. Zhou, B. Yang, W. Zhang, W. Xu, S. Dong, R. Tyagi, et al. 2021. Distinct persistence fate of *Mycobacterium tuberculosis* in various types of cells. *mSystems* 6 (4): e0078321. https://doi.org/10.1128/mSystems.00783-21.

Deghmane, A.E., H. Soualhine, H. Bach, K. Sendide, S. Itoh, A. Tam, S. Noubir, A. Talal, R. Lo, S. Toyoshima, et al. 2007. Lipoamide dehydrogenase mediates retention of coronin-1 on BCG vacuoles, leading to arrest in phagosome maturation. *Journal of Cell Science* 120 (Pt 16): 2796–2806. https://doi.org/10.1242/jcs.006221.

Dengjel, J., O. Schoor, R. Fischer, M. Reich, M. Kraus, M. Muller, K. Kreymborg, F. Altenberend, J. Brandenburg, H. Kalbacher, et al. 2005. Autophagy promotes MHC class II presentation of peptides from intracellular source proteins. *Proc Natl Acad Sci U S A* 102 (22): 7922–7927. https://doi.org/10.1073/pnas.0501190102.

Ernst, J.D. 2012. The immunological life cycle of tuberculosis. *Nature Reviews Immunology* 12 (8): 581–591. https://doi.org/10.1038/nri3259.

Fang, J., C. Dong, and S. Xiong. 2022. *Mycobacterium tuberculosis* Rv0790c inhibits the cellular autophagy at its early stage and facilitates mycobacterial survival. *Frontiers in Cellular and Infection Microbiology* 12: 1014897. https://doi.org/10.3389/fcimb.2022.1014897.

Flannagan, R.S., V. Jaumouille, and S. Grinstein. 2012. The cell biology of phagocytosis. *Annual Review of Pathology: Mechanisms of Disease* 7: 61–98. https://doi.org/10.1146/annurev-pathol-011811-132445.

Franco, L.H., V.R. Nair, C.R. Scharn, R.J. Xavier, J.R. Torrealba, M.U. Shiloh, and B. Levine. 2017. The ubiquitin ligase Smurf1 functions in selective autophagy of *Mycobacterium tuberculosis* and anti-tuberculous host defense. *Cell Host & Microbe* 21 (1): 59–72. https://doi.org/10.1016/j.chom.2016.11.002.

Ge, P., Z. Lei, Y. Yu, Z. Lu, L. Qiang, Q. Chai, Y. Zhang, D. Zhao, B. Li, Y. Pang, et al. 2022. *M. tuberculosis* PknG manipulates host autophagy flux to promote pathogen intracellular survival. *Autophagy* 18 (3): 576–594. https://doi.org/10.1080/15548627.2021.1938912.

Gomes, L.C., and I. Dikic. 2014. Autophagy in antimicrobial immunity. *Molecular Cell* 54 (2): 224–233. https://doi.org/10.1016/j.molcel.2014.03.009.

Gomez-Sanchez, R., J. Rose, R. Guimaraes, M. Mari, D. Papinski, E. Rieter, W.J. Geerts, R. Hardenberg, C. Kraft, C. Ungermann, et al. 2018. Atg9 establishes Atg2-dependent contact sites between the endoplasmic reticulum and phagophores. *Journal of Cell Biology* 217 (8): 2743–2763. https://doi.org/10.1083/jcb.201710116.

Gutierrez, M.G., S.S. Master, S.B. Singh, G.A. Taylor, M.I. Colombo, and V. Deretic. 2004. Autophagy is a defense mechanism inhibiting BCG and *Mycobacterium tuberculosis* survival in infected macrophages. *Cell* 119 (6): 753–766. https://doi.org/10.1016/j.cell.2004.11.038.

Huang, D., and L. Bao. 2016. *Mycobacterium tuberculosis* EspB protein suppresses interferon-gamma-induced autophagy in murine macrophages. *Journal of Microbiology, Immunology, and Infection* 49 (6): 859–865. https://doi.org/10.1016/j.jmii.2014.11.008.

Huang, J., and J.H. Brumell. 2014. Bacteria-autophagy interplay: A battle for survival. *Nature Reviews Microbiology* 12 (2): 101–114. https://doi.org/10.1038/nrmicro3160.

Jain, P., T. Hsu, M. Arai, K. Biermann, D.S. Thaler, A. Nguyen, P.A. Gonzalez, J.M. Tufariello, J. Kriakov, B. Chen, et al. 2014. Specialized transduction designed for precise high-throughput unmarked deletions in *Mycobacterium tuberculosis*. *Mbio* 5 (3): e01245–e11214. https://doi.org/10.1128/mBio.01245-14.

Kim, J., M. Kundu, B. Viollet, and K.L. Guan. 2011. AMPK and mTOR regulate autophagy through direct phosphorylation of Ulk1. *Nature Cell Biology* 13 (2): 132–141. https://doi.org/10.1038/ncb2152.

Lei, Y., X. Cao, W. Xu, B. Yang, Y. Xu, W. Zhou, S. Dong, Q. Wu, K. Rahman, R. Tyagi, et al. 2021. Rv3722c promotes *Mycobacterium tuberculosis* survival in macrophages by interacting with TRAF3. *Frontiers in Cellular and Infection Microbiology* 11: 627798. https://doi.org/10.3389/fcimb.2021.627798.

Liang, M., Z. Habib, K. Sakamoto, X. Chen, and G. Cao. 2017. Mycobacteria and autophagy: Many questions and few answers. *Current Issues in Molecular Biology* 21: 63–72. https://doi.org/10.21775/cimb.021.063.

Lutz, M.B., N. Kukutsch, A.L. Ogilvie, S. Rossner, F. Koch, N. Romani, and G. Schuler. 1999. An advanced culture method for generating large quantities of highly pure dendritic cells from mouse bone marrow. *Journal of Immunological Methods* 223 (1): 77–92. https://doi.org/10.1016/s0022-1759(98)00204-x.

Manzanillo, P.S., J.S. Ayres, R.O. Watson, A.C. Collins, G. Souza, C.S. Rae, D.S. Schneider, K. Nakamura, M.U. Shiloh, and J.S. Cox. 2013. The ubiquitin ligase parkin mediates resistance to intracellular pathogens. *Nature* 501 (7468): 512–516. https://doi.org/10.1038/nature12566.

Matsunaga, K., T. Saitoh, K. Tabata, H. Omori, T. Satoh, N. Kurotori, I. Maejima, K. Shirahama-Noda, T. Ichimura, T. Isobe, et al. 2009. Two Beclin 1-binding proteins, Atg14L and Rubicon, reciprocally regulate autophagy at different stages. *Nature Cell Biology* 11 (4): 385–396. https://doi.org/10.1038/ncb1846.

Mcdonough, K.A., Y. Kress, and B.R. Bloom. 1993. Pathogenesis of tuberculosis: Interaction of *Mycobacterium tuberculosis* with macrophages. *Infection and Immunity* 61 (7): 27c63–2773. https://doi.org/10.1128/iai.61.7.2763-2773.1993.

Mehra, A., A. Zahra, V. Thompson, N. Sirisaengtaksin, A. Wells, M. Porto, S. Koster, K. Penberthy, Y. Kubota, A. Dricot, et al. 2013. *Mycobacterium tuberculosis* type VII secreted effector EsxH targets host ESCRT to impair trafficking. *PLoS Pathogens* 9 (10): e1003734. https://doi.org/10.1371/journal.ppat.1003734.

Paz, I., M. Sachse, N. DuPont, J. Mounier, C. Cederfur, J. Enninga, H. Leffler, F. Poirier, M.C. Prevost, F. Lafont, et al. 2010. Galectin-3, a marker for vacuole lysis by invasive pathogens. *Cellular Microbiology* 12 (4): 530–544. https://doi.org/10.1111/j.1462-5822.2009.01415.x.

Poirier, V., Av-Gay, Y., 2015. Intracellular growth of bacterial pathogens: the role of secreted effector proteins in the control of phagocytosed microorganisms. *Microbiol Spectr* 3 (6). https://doi.org/10.1128/microbiolspec.VMBF-0003-2014.

Rabanal-Ruiz, Y., E.G. Otten, and V.I. Korolchuk. 2017. mTORC1 as the main gateway to autophagy. *Essays in Biochemistry* 61 (6): 565–584. https://doi.org/10.1042/EBC20170027.

Rahman, K., M. Jamal, X. Chen, W. Zhou, B. Yang, Y. Zou, W. Xu, Y. Lei, C. Wu, X. Cao, et al. 2022. Reprogramming *Mycobacterium tuberculosis* CRISPR System for gene editing and genome-wide RNA interference Screening. *Genomics, Proteomics & Bioinformatics* 20 (6): 1180–1196. https://doi.org/10.1016/j.gpb.2021.01.008.

Reheman, A., Cao, X., Wang, Y., Nie, X., Cao, G., Zhou, W., Yang, B., Lei, Y., Zhang, W., Naeem, M.A., et al., 2023. Involvement of 2′-5′ oligoadenylate synthetase-like protein in the survival of *Mycobacterium tuberculosis* avirulent strain in macrophages. *Animal Diseases* 3(5). https://doi.org/10.1186/s44149-023-00068-w.

Romagnoli, A., M.P. Etna, E. Giacomini, M. Pardini, M.E. Remoli, M. Corazzari, L. Falasca, D. Goletti, V. Gafa, R. Simeone, et al. 2012. ESX-1 dependent impairment of autophagic flux by *Mycobacterium tuberculosis* in human dendritic cells. *Autophagy* 8 (9): 1357–1370. https://doi.org/10.4161/auto.20881.

Saini, N.K., A. Baena, T.W. Ng, M.M. Venkataswamy, S.C. Kennedy, S. Kunnath-Velayudhan, L.J. Carreno, J. Xu, J. Chan, M.H. Larsen, et al. 2016. Suppression of autophagy and antigen presentation by *Mycobacterium tuberculosis* PE_PGRS47. *Nature Microbiology* 1 (9): 16133. https://doi.org/10.1038/nmicrobiol.2016.133.

Sala, C., N.T. Odermatt, P. Soler-Arnedo, M.F. Gulen, S. Von Schultz, A. Benjak, and S.T. Cole. 2018. EspL is essential for virulence and stabilizes EspE, EspF and EspH levels in *Mycobacterium tuberculosis*. *PLoS Pathogens* 14 (12): e1007491. https://doi.org/10.1371/journal.ppat.1007491.

Schmid, D., M. Pypaert, and C. Munz. 2007. Antigen-loading compartments for major histocompatibility complex class II molecules continuously receive input from autophagosomes. *Immunity* 26 (1): 79–92. https://doi.org/10.1016/j.immuni.2006.10.018.

Strong, E.J., T.W. Ng, S.A. Porcelli, and S. Lee. 2021. *Mycobacterium tuberculosis* PE_PGRS20 and PE_PGRS47 Proteins Inhibit Autophagy by Interaction with Rab1A. *mSphere* 6 (4): e0054921. https://doi.org/10.1128/mSphere.00549-21.

Stroupe, C. 2018. This is the end: Regulation of Rab7 nucleotide binding in endolysosomal trafficking and autophagy. *Front Cell Dev Biol* 6: 129. https://doi.org/10.3389/fcell.2018.00129.

Sun, Q., J. Zhang, W. Fan, K.N. Wong, X. Ding, S. Chen, and Q. Zhong. 2011. The RUN domain of rubicon is important for hVps34 binding, lipid kinase inhibition, and autophagy suppression. *Journal of Biological Chemistry* 286 (1): 185–191. https://doi.org/10.1074/jbc.M110.126425.

Suzuki, K., M. Akioka, C. Kondo-Kakuta, H. Yamamoto, and Y. Ohsumi. 2013. Fine mapping of autophagy-related proteins during autophagosome formation in *Saccharomyces cerevisiae*. *Journal of Cell Science* 126 (Pt 11): 2534–2544. https://doi.org/10.1242/jcs.122960.

Tamura, N., T. Nishimura, Y. Sakamaki, I. Koyama-Honda, H. Yamamoto, and N. Mizushima. 2017. Differential requirement for ATG2A domains for localization to autophagic membranes and lipid droplets. *FEBS Letters* 591 (23): 3819–3830. https://doi.org/10.1002/1873-3468.12901.

Turco, E., D. Fracchiolla, and S. Martens. 2020. Recruitment and activation of the ULK1/Atg1 kinase complex in selective autophagy. *Journal of Molecular Biology* 432 (1): 123–134. https://doi.org/10.1016/j.jmb.2019.07.027.

Velikkakath, A.K., T. Nishimura, E. Oita, N. Ishihara, and N. Mizushima. 2012. Mammalian Atg2 proteins are essential for autophagosome formation and important for regulation of size and distribution of lipid droplets. *Molecular Biology of the Cell* 23 (5): 896–909. https://doi.org/10.1091/mbc.E11-09-0785.

Vergne, I., J. Chua, H.H. Lee, M. Lucas, J. Belisle, and V. Deretic. 2005. Mechanism of phagolysosome biogenesis block by viable *Mycobacterium tuberculosis*. *Proc Natl Acad Sci U S A* 102 (11): 4033–4038. https://doi.org/10.1073/pnas.0409716102.

GPP Web Portal [Online]. Broad Institute. Available: https://portals.broadinstitute.org/gpp/public/gene/search. Accessed 11 June 2021.

Wong, K.W., 2017. The Role of ESX-1 in *Mycobacterium tuberculosis* Pathogenesis. *Microbiol Spectr* 5 (3). https://doi.org/10.1128/microbiolspec.TBTB2-0001-2015.

Xu, J., O. Laine, M. Masciocchi, J. Manoranjan, J. Smith, S.J. Du, N. Edwards, X. Zhu, C. Fenselau, and L.Y. Gao. 2007. A unique *Mycobacterium* ESX-1 protein cosecretes with CFP-10/ESAT-6 and is necessary for inhibiting phagosome maturation. *Molecular Microbiology* 66 (3): 787–800. https://doi.org/10.1111/j.1365-2958.2007.05959.x.

Yang, F., Y. Lei, M. Zhou, Q. Yao, Y. Han, X. Wu, W. Zhong, C. Zhu, W. Xu, R. Tao, et al. 2018. Development and application of a recombination-based library versus library high-throughput yeast two-hybrid (RLL-Y2H) screening system. *Nucleic Acids Research* 46 (3): e17. https://doi.org/10.1093/nar/gkx1173.

Yu, L., Y. Chen, and S.A. Tooze. 2018. Autophagy pathway: Cellular and molecular mechanisms. *Autophagy* 14 (2): 207–215. https://doi.org/10.1080/15548627.2017.1378838.

Zachari, M., and I.G. Ganley. 2017. The mammalian ULK1 complex and autophagy initiation. *Essays in Biochemistry* 61 (6): 585–596. https://doi.org/10.1042/EBC20170021.

Zaffagnini, G., and S. Martens. 2016. Mechanisms of Selective Autophagy. *Journal of Molecular Biology* 428 (9 Pt A): 1714–1724. https://doi.org/10.1016/j.jmb.2016.02.004.

Publisher's Note